Bioinspiration & Biomimetics

OPEN ACCESS

RECEIVED
10 January 2022

REVISED
1 March 2022

ACCEPTED FOR PUBLICATION
8 March 2022

PUBLISHED
10 May 2022

PAPER

Self-organized rod undulations on pre-stretched textiles

Lorenzo Guiducci[1,3,*], **Agata Kycia**[2], **Christiane Sauer**[1,2], **and Peter Fratzl**[1,3]

[1] Humboldt-Universität zu Berlin, Cluster of Excellence 'Matters of Activity. Image Space Material', Unter den Linden 6, 10099 Berlin, Germany
[2] Department of Textile and Surface Design, Weissensee Kunsthochschule Berlin, Germany, Bühringstraße 20, Berlin 13086, Germany
[3] Department of Biomaterials, Max Planck Institute of Colloids and Interfaces, Am Mühlenberg 1, Potsdam 14476, Germany
[*] Author to whom any correspondence should be addressed.

E-mail: lorenzo.guiducci@mpikg.mpg.de

Keywords: 4D textiles, rod-membrane assemblies, differential strain, surface texturing, 3D printing on pre-stretched textiles, self-shaping textiles, form finding

Supplementary material for this article is available online

Abstract

Textile technology is a traditional approach to additive manufacturing based on one-dimensional yarn. Printing solid rods onto pre-stretched textiles creates internal stresses upon relaxation of the pre-stretch, which leads to buckling-induced out-of-plane deformation of the textile. Similar behaviours are well known to occur also in biological systems where differential growth leads to internal stresses that are responsible for the folding or wrinkling of leaves, for example. Our goal was to get a quantitative understanding of this wrinkling by a systematic experimental and numerical investigation of parallel rods printed onto a pre-stretched textile. We vary rod thickness and spacing to obtain wavelength and phase coherence of the wrinkles as a function of these parameters. We also derive a simple analytical description to rationalize these observations. The result is a simple analytical estimate for the phase diagram of behaviours that may be used for design purposes or to describe wrinkling phenomena in biological or bioinspired systems.

1. Introduction

Compared with engineering materials, biological materials are characterized by a limited number of chemical elements, but a much greater complexity and variability of their internal structure (Fratzl and Weinkamer 2007). Wood and bone are perfect examples of strong, tough, yet lightweight materials ('shape cheap, materials expensive' in Julian Vincent's effective words https://smartgeometry.org/shape-cheap-materials-expensive). Owing to the numerous structure–function relationships discovered in the last decade, engineers and materials scientists now consider biological materials as a rich repository of exemplary solutions to devise new structural, multifunctional and programmable materials. In the realm of architecture and design, advanced materials research, fast-improving computational design tools and additive manufacturing technologies (nowadays capable of scale-bridging and multi-material fabrication) have led to new form-finding processes that tap into the biological realm for inspiration and a sustainable approach to material deployment. These novel perspectives enable an unprecedented liberty in the design process, in the best spirit of Frei Otto's legacy (Otto and Rasch 1995).

In particular, studies on morphogenetic processes in both living and non-living thin tissues such as leaves, flowers and plastic foils (Sharon *et al* 2002, Pocivavsek *et al* 2008, Liang and Mahadevan 2009), or the relatively new field of 3D printing on textiles (Guberan and Clopath 2016) testify the convergence of research interests and techniques towards materials and form by natural scientists, architects and designers alike. A fast, reproducible and inexpensive prototyping technique, 3D printing on pre-stretched elastic textiles has posed a link between three dimensional computational designs and physical models, establishing digital manufacturing workflows that are less affected by intrinsic error sources and -in principle- more scalable. Nevertheless programing a 3D shape into a flat stretched textile is not a trivial task.

In geometrical terms, the rigid pattern imposes an intrinsic metric onto the textile surface which might not be embeddable in the Euclidean space (Sharon and Efrati 2010). In practical terms this means that the final rest state is not unique and many 3D configurations are possible.

Therefore a big part of the literature has focussed on solving the so-called inverse design problem, that is how to reverse engineer a target three-dimensional shape into the layout of a 2D material system. This problem has been approached in a few ways: by subdividing the target surface in a patchwork of stiff rods enclosing smaller textile patches under tension (Perez *et al* 2017), or by programing the textile contraction upon tension release through a pattern of rigid hexagonal tesserae of varying size (Nervous Studio). Other interesting studies (Jourdan *et al* 2020) explored the design space of textiles covered with star-shaped elements, taking into account variations of geometrical quantities and physical effects (such as the offset of printed rods with respect to the fabric plane).

While the majority of these studies are of great relevance for applied research in design and architecture as they provide computational tools to achieve a target 3D shape, they miss to deliver a comprehensive understanding of the morphing mechanism in self-shaping textiles with rods-on-membrane designs (that is when the fused filament is deposited onto the textile into single, non-intersecting lines). Therefore in this contribution we study the morphing behaviour of the most basic rods-on-membrane geometric pattern, namely straight parallel lines, focussing on the undulations obtained after tension release. We use a combination of physical, finite element (FE) and analytical modelling to systematically explore the design space (for experimental details, see supplementary material (https://stacks.iop.org/BB/17/036007/mmedia)). In doing so, we uncover the mechanism by which the main geometric parameters influence the morphing process. Finally, we also build larger self-shaping textile prototypes to demonstrate possible application scenarios.

2. Undulations of 3D printed thin rods on pre-stretched membrane

We start by assessing the influence of rod thickness h and fabric pre-strain ε_0 in single 3D printed straight rods. Due to the thin cross section of the rods (as thin as $h = 0.1$ mm) and the strong knitted elastic textile used ($E = 0.45$ MPa, thickness $t = 0.4$ mm), upon tension release the rods buckle out of plane into an undulated configuration resembling a series of circular arcs (described by the arc length l, wavelength λ, amplitude a, radius of curvature R in figure 1). This is similar, but not identical, to the sinusoidal buckling mode (wrinkling) observed in a thin film bonded to a soft substrate (Bowden *et al* 1998, Cerda and Mahadevan 2003, Brau *et al* 2013). We attribute this circular arc geometry to the bilayer architecture of the rod-fabric assembly (as rods and fabric have comparable thickness) which is well described by the theory of spontaneous curvature in thin bilayers with strain mismatch (Timoshenko 1925). We observe that increasing the rod's thickness at same textile pre-stretch results into larger wavy shapes (figure 1(b), left). Instead, changing the pre-strain at constant rod thickness has little influence on the wave profile shape (figure 1(b), right): increasing (decreasing) it results in slightly smaller (larger) wavelengths and higher (lower) amplitudes. While this is similar to the accordion model deformation observed in the 1D wrinkling of hard films on soft substrate systems our data suggests that the number of half waves per initial length of the rod depends weakly on the pre-strain (in contrast with the accordion model which assumes that it does not change in the post-buckling regime) (Jiang *et al* 2007).

3. Finite element model of rod-on-membrane

To bypass the limitations and inaccuracies of the 3D printing process, we resolved to a FE model (see supplementary material—FE model) to probe the effect of rod thickness with a much higher granularity than achievable with our 3D printing setup ($h = [0.08, 2.0]$ mm in 0.02 mm steps). As the tension on the fabric boundary is gradually released, the fabric shrinks in plane until the rod buckles out of plane. We notice the existence of a well defined critical strain (at about $\varepsilon_0 \cong 0.35$ engineering strain in all cases) where buckling starts, which is smaller than the one introduced by pre-stretching the fabric. Because of this, releasing the tension on the fabric always overcomes the critical strain and leads to the formation of waves. Since the textile exerts a non-uniform compression on the rod (larger at the centre than at the extremities), the undulated pattern appears first in the rod central portion and propagates outwards towards the rod ends. Once the tension on the fabric is completely released the rod assumes a uniform wavy shape, except for the two ends which show a lower curvature (figure 1(a)). While in all our simulated cases this boundary effect is confined to the two peripheral half waves, in theory it could propagate further inside, localizing in the central portion of the rod, as reported for filaments adhered on a thick substrate with very low shear modulus (Michaels 2019). The deformed rod shapes computed through FE match very closely those observed in the physical models. In almost all simulated cases, the rods assume a wave shape with an odd number of circular segments, according with the mirror symmetry of the system at the rod midsection. The segments

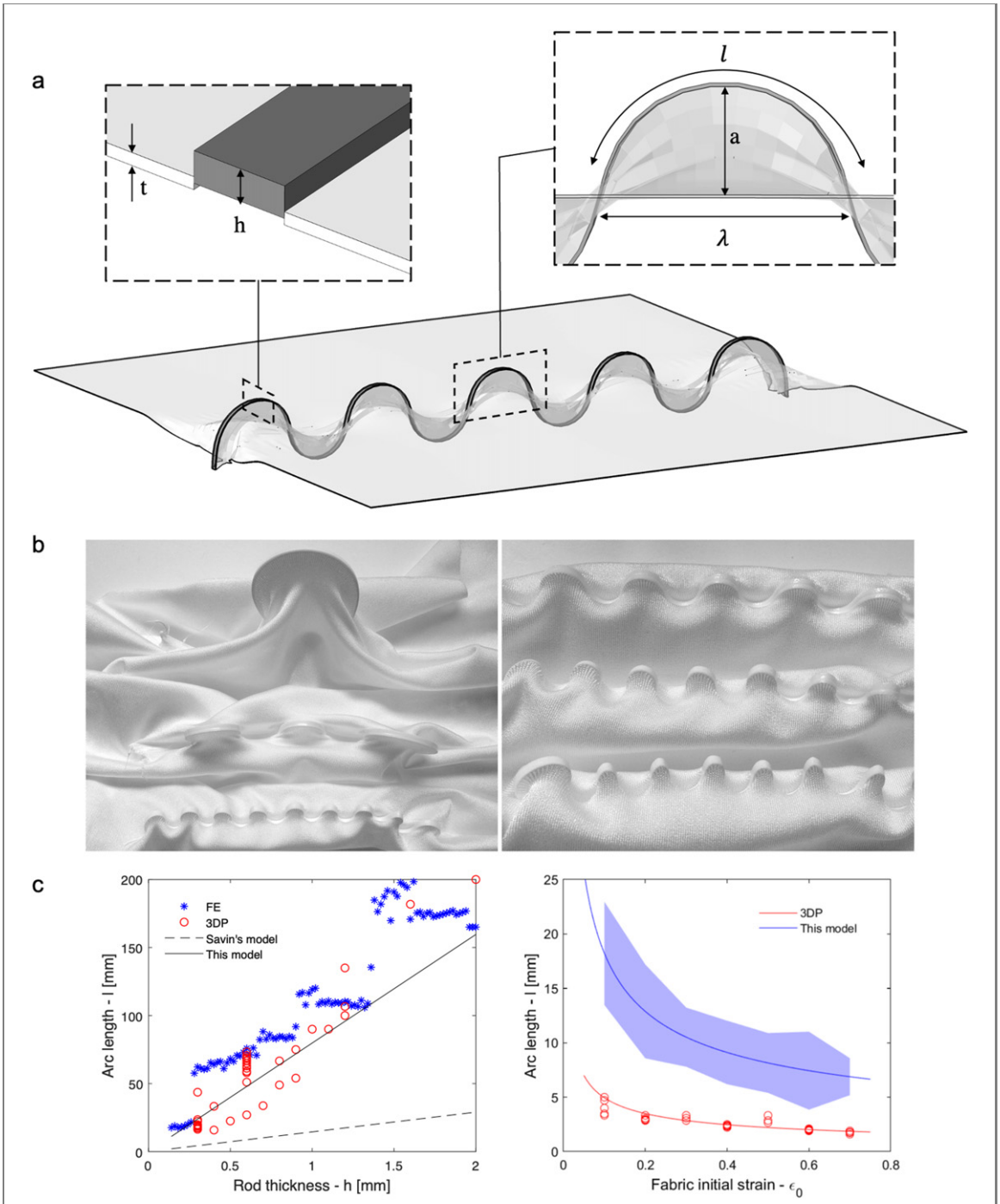

Figure 1. (a) Geometry of the single buckled rod, with magnified views on rod's cross section and half wave. (b) Left, from bottom to top: large increase in waves size with increasing rod thickness; right, from bottom to top: minor increase in waves size with decreasing fabric pre-stretch. (c) Left: linear dependence of half wave arc length l to rod thickness h in a single buckled rod (blue: FE data; red: physical models; solid line: the proposed analytical model; dashed line: scaling law from Savin *et al* 2011); right: half wave arc length shows inverse square root proportionality to the pre-strain $l \propto \varepsilon_0^{-1/2}$ (red circles: measured arc length in physical models; red line: best fit of measured arc length using equation (1), with $h = 0.04$ mm; blue line: model prediction using rod thickness mean value $h = 0.147$ mm; blue shaded area indicates variations in model prediction due to rod thickness measurement error—calculated as standard deviation).

in the top half space (taking the initial fabric plane as reference) have consistently slightly higher curvature than those in the bottom half. This results from the up-down asymmetry of the system (since rods are bonded on top of the fabric, the rod cross-section is offset with respect to the fabric plane), which amplifies the rod curvature when the fabric is at the convex side by the aforementioned bilayer effect.

The resulting deformed configuration of the rod at rest state is analysed by fitting the nodal coordinates through both a sine wave and a series of circular arcs. Fitting with circular arcs resulted in the lowest residuals throughout the dataset and an R^2 value close to 1, confirming our observations of the physical models (see supplementary material—shape analysis and fitting).

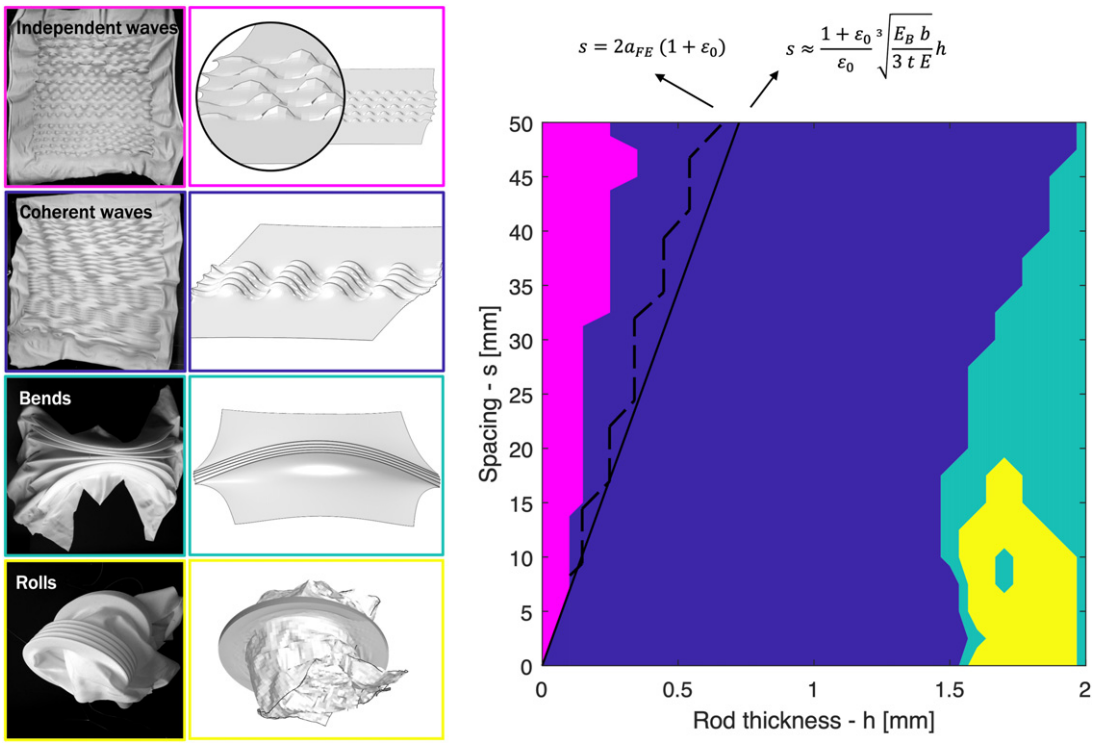

Figure 2. A phase diagram of rods-on-fabric buckled shapes in the h–s space (h, rod thickness; s, rod–rod spacing) and corresponding shapes (left: physical models; right: FE model). Pink: independent waves; blue: coherent waves; green: bends; yellow: rolls. Estimates for the transition between coherent and incoherent phase $s = 2a\,(1+\varepsilon_0)$ are plotted in solid black (analytical model) and dashed black lines (FE data).

4. Analytical model of rod-on-membrane buckling

These observations motivated us to propose an alternative model of rod buckling and wave formation specific for rod-on-membrane systems. Here we assume zero transverse tension, since the textile is free to shrink perpendicularly to the rod, neglecting second order contributions (i.e. transverse tension is locally non-zero adjacent to the rod, but has zero average over the rod length). Under simplifying assumptions of rod inextensibility and planar buckled state we approximate the shape of the buckled rod as a succession of identical circle segments (see supplementary material—analytical derivation of wave configuration) and derive an estimate of the length of the circular arc l as:

$$l = \left(24\sqrt{6}\frac{E_B I_B}{Et}\right)^{1/3} \varepsilon_0^{-1/2}. \qquad (1)$$

Where $I_B = \frac{1}{12}h^3 b$ is the second moment of area of the rod rectangular cross section. We notice that equation (1) has similar scaling to the wavelength in a film attached to a soft substrate (equation (25) in Brau *et al* 2013). In our model the arc length scales linearly with the rod thickness h, in agreement with both the experimental and FE data, although at large values of thickness h the FE data clusters around discrete arc length values (figure 1(c) left). Even more interestingly, there is an inverse proportionality to the square root of the pre-strain ε_0 (figure 1(c) right) also in agreement with our experimental and FE data, thus confirming the inherently different mechanics at play in this class of systems -rod on membrane- compared with film on substrate systems. The system analysed here shares similar geometry (and mechanics) with the embryogenesis of gut tube and attached mesentery in many animal species, which develops characteristic circular loops (Savin *et al* 2011). In our case the rod has a rectangular cross-section, which helps stabilizing against twisting and preserves the planarity of the buckled rod. While the treatment of gut looping by Savin *et al* produces similar scaling laws ($l \propto \left(\frac{E_B I_B}{Et}\right)^{1/3}$), our model additionally specifies exact coefficients and is in good agreement with our experimental and FE data.

5. A phase diagram for parallel rods

With outlook towards architectural applications, multiple lines are needed to realize surface coverage and panelling. In its most simple realization, surface coverage can be obtained by a collection of parallel straight lines. To this end, we study the morphing behaviour of N parallel straight lines as a natural extension to the single rod case treated so far. The geometry of the problem is similar to the one treated by Wu (Wu *et al* 2013) for a micrometre thick monolayer consisting of two hydrogels with

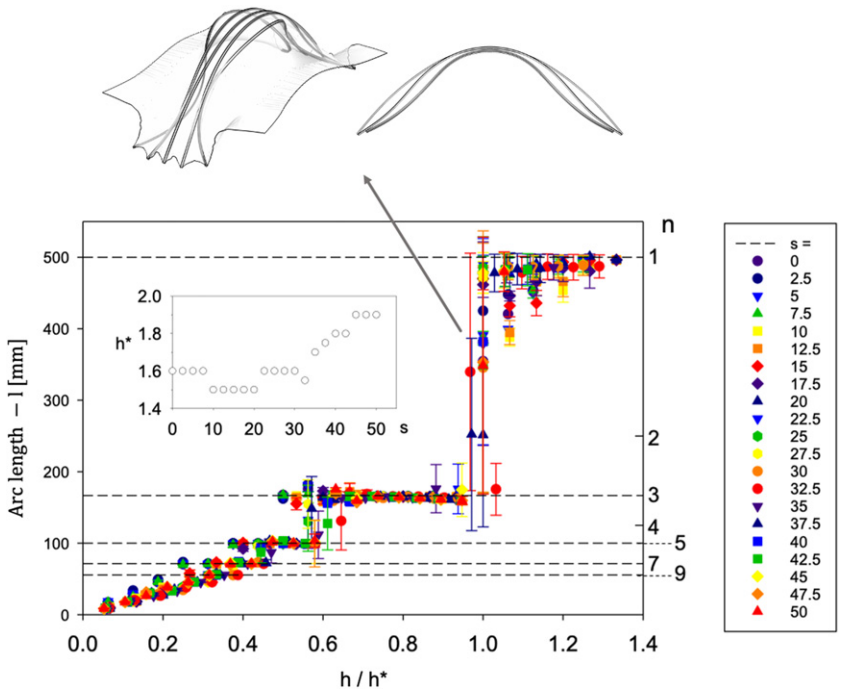

Figure 3. Half wave arc length at different rod thickness h and rod–rod spacing (FE data). Each point in the plot represents a single FE simulation. The abscissa is rescaled by the value of rod thickness at the 3 −> 1 transition (h^*). h^* is determined empirically and shown in the inset as a function of line spacing s. At low values of h/h^* the relationship is linear; at larger values of h/h^* the arc length clusters around discrete levels corresponding to an odd number of half waves (indicated by the secondary axis). Close to transition points the arc length data is more scattered (larger error bars): here equilibrium states with different number of half waves in the rods occur (image refers to $h = 1.8$ mm, $s = 40$ mm at 3 −> 1 transition point).

contrasting swelling coefficients and elastic moduli arranged in a banded pattern.

We build a FE model comprising $N = 5$ parallel lines centred in the fabric and run a large parametric study covering the two main geometric parameters in the design space, namely rod thickness h, and initial rod–rod spacing s in the interval $[h, s] = [0.1, 2.0] \times [0, 50]$, with $\Delta h = 0.1$, $\Delta s = 2.5$ for a total of 420 simulations. In all cases the textile morphed similarly to the single line case: as the tension in the fabric is released the fabric first shrinks, then the rods buckle out of plane. Generally, the peripheral rods reach the instability earlier, as they are compressed by a larger portion of fabric than the internal rods (see supplementary material—FE model). The shape analysis of the buckled rods revealed four different shape families, also observed in corresponding physical models (figure 2). In the largest part of the h–s phase diagram (at intermediate h and all s values) the rods reach a buckled state characterized by waves that are in phase (coherent waves). At very low h and large s the rods buckle into independent waves (out of phase). At large h instead the rods form a single half wave that can be further differentiated into rolls (at small s, when $\lambda < 2a$) or bends (at large s, when $\lambda > 2a$). In more detail, all shape metrics considered in this study (arc length l, wavelength λ, amplitude a, radius of fitting circle R) increase with rod thickness, whereas the influence of rod–rod spacing is minor.

6. Breakdown of linear model, arc length is quantized

As for the single rod case, a departure from linearity of the shape metrics (e.g. the arc length in figure 3) can be seen as these cluster around discrete values at large thickness h.

For all values of line spacing s, the configuration at large values of the line thickness h is a single half-wave where the whole tissue is bent along a circle, approximately. The thickness h^* where this transition to the single half wave occurs depends to some extent on the line spacing s. We plot the arc length l mean value as a function of the rescaled line thickness h/h^* for all available data. Mean value and standard deviation (shown by error bars) are computed for datasets with same values of h and s (each dataset comprises $N = 5$ rods, except $N = 1$ for $s = 0$). On the right side, we indicate the values of l corresponding to L/n, where L is the total rod length and n is the number of half-waves. The insert shows the value of h^* as a function of line spacing s (determined empirically, so that the transition to the final state with $n = 1$ occurs at $h/h^* = 1$). Interestingly, at sufficiently large values of h/h^*, l is quantized according to the number of half-waves, whereby asymmetric states with even values of n only occur very occasionally in unstable regions close to a transition. Mostly l takes values of L/n with n odd (corresponding to symmetric waving or bending). At small values of h (where $n > 10$), the

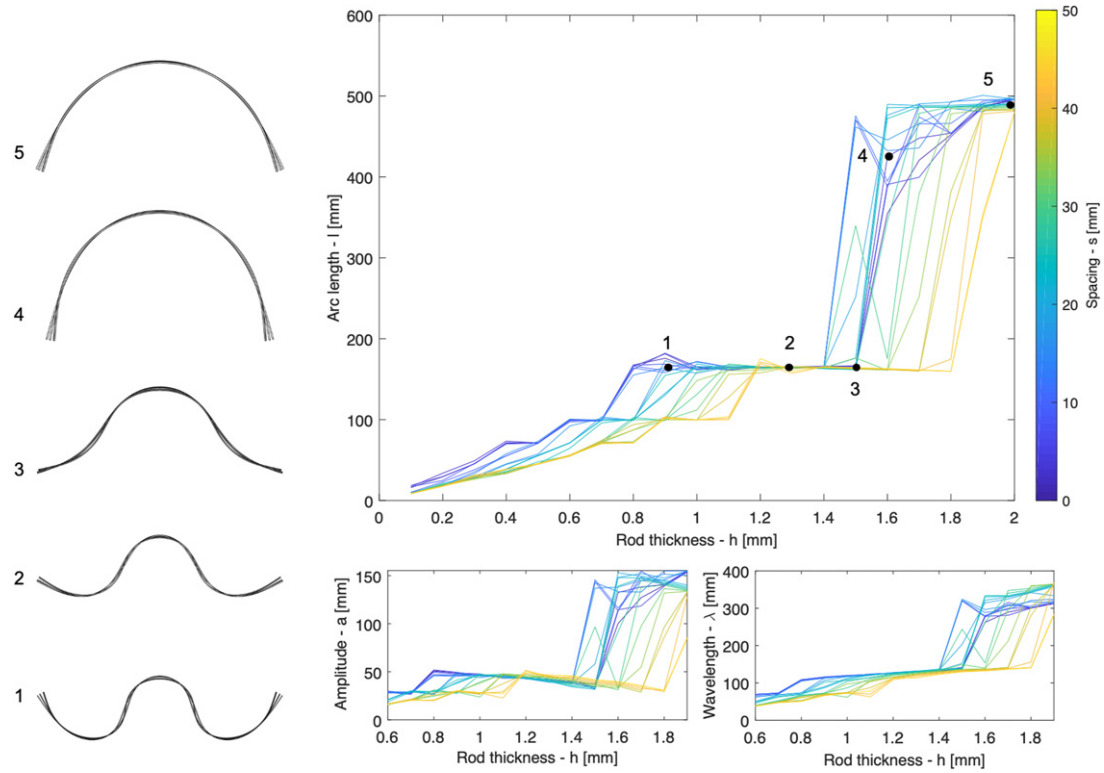

Figure 4. When the half wave arc length reaches values comparable to the total rod length, the system shifts to quantized states, characterized by a plateau in arc length. Here an increase of rods thickness results in flatter half waves (slightly decreasing amplitude and increasing wavelength—see successive states $1 \rightarrow 2 \rightarrow 3$ and $4 \rightarrow 5$) until the peripheral half waves unfold and merge with the central one (three-to-one half waves transition at states $3 \rightarrow 4$). Images at the left show equilibrium states for $s =$ 7.5 mm and $h = 0.9$ mm (1), $h = 1.3$ mm (2), $h = 1.5$ mm (3), $h = 1.6$ mm (4), $h = 2.0$ mm (5).

quantization cannot be seen anymore (or might not exist). Moreover, through the scaling of h by h^* (which encompasses the effect of spacing s), the data points end up on an almost universal master curve. Typically, the error bars are large only in the vicinity of transition points, where the system cannot 'decide' whether it 'prefers' a state corresponding to n or to $n + 2$: then the averaging of several states with different n gives an intermediate value of l and a large error bar (see figure 3 and supplementary material—waves misalignment).

In conclusion, these quantized states can be understood as finite size effects of the fabric-rod system in its buckled state, that is when the arc length l becomes comparable with the system size L. As the rod can only stably occupy a state with n (odd) half waves, the arc length is constant until the next transition point, where the peripheral half waves unfold and merge with the central one ($n + 2 \rightarrow n$). In this plateau an increase in h (and the consequent rod stiffening) causes a flattening of the half wave shape (corresponding to a decreasing amplitude and increasing wavelength—see figure 4).

7. Understanding the role of rod–rod spacing

The influence of rod–rod spacing on the buckled configuration is not self-evident. In general, its influence on all shape metrics (arc length, wavelength, amplitude, radius of curvature) is much smaller than the thickness. To highlight the role of spacing, we first discuss the two extreme cases of very large and vanishing spacing. If the lines are sufficiently far apart ($s \rightarrow \infty$) then all rods are equally compressed by two adjacent portions of fabric and the single line buckling mode is still valid. This scenario occurs in the independent waves phase (pink area in the phase diagram in figure 2). Here the spacing is larger than a characteristic length $\hat{s}$ over which the tension relaxes ($s > \hat{s}$): since the fabric tension vanishes between two rods, there is no energy penalty if the waves are not in phase. If after relaxation the fabric is tensioned only in the area subtended by a half wave (as we assumed in our analytical model) then the characteristic spacing $\hat{s}$ can be related to the wave amplitude by the condition: $\frac{\hat{s}}{1+\varepsilon_0} = 2a$. In the phase diagram we plot the contour line $s = \hat{s} = 2a\,(1 + \varepsilon_0)$ from waves amplitude values measured from the FE data (dashed line) and also using an analytical expression of the wave amplitude derived from our model $a \approx \frac{1}{2\varepsilon_0}\sqrt[3]{\frac{E_R b}{3Et}}h$ (solid line). Remarkably, these two *loci* are almost coinciding and correctly delimit the portion of phase space in which independent waves are observed.

Conversely, for small spacing ($s \rightarrow 0$) the N individual rods 'bundle' together into a single rod with N times the breadth. In terms of the rod's second

Figure 5. Self-shaping textile produced via manual deposition of polymeric adhesives into various geometric patterns of non-intersecting lines. The lines have approximately same thickness but variable spacing, orientation and number. Additional fabric tension due to gravity enrich the range of attainable surface textures with graded properties of translucency and shadow casting for an interior architectural setting.

moment of inertia, this is equivalent to scaling the rod thickness h by $\sqrt[3]{N}$ in equation (1). According to these considerations and indicating as h_s^* the critical thickness at the $n+2 \to n$ phase transition for a given spacing s, the ratio $h^*_{s=0}/h^*_{s\to\infty}$ should be in the order of $\sqrt[3]{5} \approx 1.7$ (remember the system comprises $N = 5$ rods). We derived empirically the ratio $h^*_{s=0}/h^*_{s=50}$ for the first three transitions and obtain convincingly close estimates: $3 \to 1$: 1.35; $5 \to 3$: 1.57; $7 \to 5$: 1.75. Note that these computed values become more accurate as the number of half waves n at the transition increases: clearly at lower h the waves' amplitude a decreases and therefore $s = 50 \gg \hat{s}$ which approximates well $s \to \infty$.

8. Importance of undulated self-shaping textiles for architectural settings

In order to produce self-shaping textiles with larger size than attainable with our 3D printing setup, we resolved to manual deposition of polymeric adhesives with a pneumatic glue gun (see supplementary material—upscaling printing process). Despite its intrinsic inaccuracies, this manual fabrication process resulted into formations that were qualitatively equivalent to the more precise 3D printing tests, as tolerance for errors increased together with the size and scale of the production process. The textiles were bestowed with different geometric arrangements of non-intersecting lines, approximately of same thickness but with variable spacing, orientation and number.

These prototypes have a demonstrative character and help appreciating the physical and aesthetic properties of undulated surfaces in an interior architectural setting (figure 5, left). For example, in the same textile (figure 5, centre) different patterns can be observed: the half waves cluster together into tubes, branched tubes, or stay independent. In the upper right corner of the textile, where the lines are closely spaced and align horizontally, the additional transversal tension on the fabric due to gravity results in coherent waves that appear as tubes. Since each printed line has a different length and the number of half waves is quantized, the number of half waves in neighbouring lines is incommensurate: this causes local misalignment of the waves and the tubes branch. In the central and lower portion instead, where the lines run vertically, the interstitial fabric is relaxed and we can observe the independent waves phase. Such richness of morphologies, the variable transparency caused by inhomogeneous stretch and the self-shading due to the surface texture results in peculiar overall haptic, optical or acoustical qualities (figure 5, right). These textile qualities constitute a playground for architects and designers for interior applications such as 'soft' room separators that can be programed and customized to meet specific requirements or even functional devices for the building skin.

9. Conclusions and outlook

We proposed an analytical model explaining the morphing of non-intersecting rods on a pre-stretched membrane: despite its simplicity, our model is able to capture the underlying morphing process and provide accurate estimates for the main shape metrics of the rod buckled state. In addition we elucidate the role of the system finite size and rod–rod spacing in determining the landscape of attainable shapes. This landscape is characterized by well-defined phase transitions separating different stable buckled states,

similarly to what has been proposed for other classes of architected solids (Restrepo *et al* 2015, Liu *et al* 2019, Liu *et al* 2019, Shan *et al* 2015).

While the present study helps navigate the landscape of attainable shapes, it does so under simplifying assumptions. First of all it assumes linear, elastic and isotropic properties for both rod and membrane materials. Secondly we assume that the undulations have zero mean value, that is the buckled rods essentially keep the flat state of the fabric, but a combination of global (bending) and local (wave) modes or mode switching is also possible. Unloading speed may affect the buckling mode as well, if the material is viscoelastic. In our experiments and simulations we could observe a few cases in which a rod would assume a global circular arch shape superposed to a high frequency mode, multiple superposed modes reminiscent of period doubling (Brau *et al* 2013) or even meanders characterized by circular segments with central angles larger than π. In the physical models, these modes would spontaneously appear as reconfigurations of the globally planar buckled rod, upon slight external disturbance (see supplementary material—waves reconfigurations). In the FE model these would occur by extending the simulated time period after tension relaxation where only inertial effects are present (see supplementary material—inertial effects in FE simulations). In the future it is advisable to extend the present treatment to include and specifically address these shapes, which evidently are favoured due to a lower elastic energy in the far post-buckling regime.

A possible useful development is to assess and model the effect of gravity or additional external tension, which can not only enrich the landscape of attainable shapes (as shown in figure 5) modulating the basic morphing rules introduced here, but also be relevant for real architectural applications such as canopies or pavilions (Kojima 2011). The buckled filaments integrated in our textiles result in a new architectural hybrid and dynamic element that combines flexibility and stiffness in its very surface, thus making frames and bracings obsolete, for example, in textile screen applications. These lightweight systems can be easily deployed in space and can be designed to exhibit programmable tactile, optical or acoustical properties through their specific surface modulation. The flexibility of the system even allows for further modulation and adaptation by the user through partial or overall tensioning or releasing of the membrane. Thus a functional architectural device can be created that minimizes material use and controls movement through geometry—just like we find in nature.

The peculiar non intersecting, infinite, continuous line design that we propose here prompts to a facile upscaling of their production: in the future we envision integrating out-of-the-roll, continuous-line-printing on a uniaxially stretched bolt of fabric at the textile production site. This can result in an industrialized process and architectural scaled façade or canopy elements.

In conclusion, we have shown how a simple and relatively well studied system of filament printing on textile membrane exhibits specificities that can be appealing in architectural and design contexts. We believe that our study might result inspirational for communities of architects and product designers that would like to explore material-based form finding techniques but are not invested in the physics of morphogenetic processes.

Conflict of interest

The authors have no conflicts of interest to declare that are relevant to the content of this article.

Acknowledgments

The author acknowledges the support of the Cluster of Excellence 'Matters of Activity. Image Space Material' funded by the Deutsche Forschungsgemeinschaft (DFG, German Research Foundation) under Germany's Excellence Strategy—EXC 2025—390648296.

Data availability statement

The data that support the findings of this study are available upon reasonable request from the authors.

ORCID iDs

Lorenzo Guiducci https://orcid.org/0000-0001-5104-7245

References

Bowden N, Brittain S, Evans A G, Hutchinson J W and Whitesides G M 1998 Spontaneous formation of ordered structures in thin films of metals supported on an elastomeric polymer *Nature* **393** 146–9

Brau F, Damman P, Diamant H and Witten T A 2013 Wrinkle to fold transition: influence of the substrate response *Soft Matter* **9** 8177–86

Cerda E and Mahadevan L 2003 Geometry and physics of wrinkling *Phys. Rev. Lett.* **90** 074302

Fratzl P and Weinkamer R 2007 Nature's hierarchical materials *Prog. Mater. Sci.* **52** 1263–334

Gabe Fields (Nervous Studio) 2010 https://n-e-r-v-o-u-s.com/blog/?p=8011 (accessed 22 March 2022)

Guberan C and Clopath C 2016 Active shoes (MIT Self-Assembly Lab) https://selfassemblylab.mit.edu/active-shoes

Jiang H, Khang D-Y, Song J, Sun Y, Huang Y and Rogers J A 2007 Finite deformation mechanics in buckled thin films on compliant supports *Proc. Natl Acad. Sci. USA* **104** 15607–12

Jourdan D *et al* 2020 Printing-on-fabric meta-material for self-shaping architectural models *Advances in Architectural Geometry 2020*

Kojima K 2011 https://c-and-a.co.jp/en/projects/moom/

Liang H and Mahadevan L 2009 The shape of a long leaf *Proc. Natl Acad. Sci. USA* **106** 22049–54

Liu J, Liu W, Pantula A, Wang Z, Gracias D H and Nguyen T D 2019 Periodic buckling of soft 3D printed bioinspired tubes *Extreme Mech. Lett.* **30** 100514

Liu Y, Cao Y, Feng X-Q and Cao C 2019 Phase transition and optimal actuation of active bilayer structures *Extreme Mech. Lett.* **29** 100467

Michaels T C T, Kusters R, Dear A J, Storm C, Weaver J C and Mahadevan L 2019 Geometric localization in supported elastic struts *Proc. R. Soc.* A **475** 20190370

Otto F and Rasch B 1995 Finding form—on the way to an architecture of the minimal *Finding Form: Towards an Architecture of the Minimal* (Germany: Edition Axel Menges)

Perez J, Otaduy M A and Thomaszewski B 2017 Computational design and automated fabrication of Kirchhoff-plateau surfaces *ACM Trans. Graph.* **36** 62:1–62:12

Pocivavsek L, Dellsy R, Kern A, Johnson S, Lin B, Lee K Y C and Cerda E 2008 Stress and fold localization in thin elastic membranes *Science* **320** 912–6

Restrepo D, Mankame N D and Zavattieri P D 2015 Phase transforming cellular materials *Extreme Mech. Lett.* **4** 52–60

Savin T, Kurpios N A, Shyer A E, Florescu P, Liang H, Mahadevan L and Tabin C J 2011 On the growth and form of the gut *Nature* **476** 57–62

Shan S, Kang S H, Raney J R, Wang P, Fang L, Candido F, Lewis J A and Bertoldi K 2015 Multistable architected materials for trapping elastic strain energy *Adv. Mater.* **27** 4296–301

Sharon E and Efrati E 2010 The mechanics of non-Euclidean plates *Soft Matter* **6** 5693–704

Sharon E, Roman B, Marder M, Shin G-S and Swinney H L 2002 Buckling cascades in free sheets *Nature* **419** 579

Timoshenko S 1925 Analysis of bi-metal thermostats *J. Opt. Soc. Am.* **11** 233–55

Wu Z L *et al* 2013 Three-dimensional shape transformations of hydrogel sheets induced by small-scale modulation of internal stresses *Nat. Commun.* **4** 1–7